Fully Automated Radiogrammetric Measurement of Third Metacarpal Bone from Hand Radiograph

*Anu Shaju Areeckal, *Sumam David S, †Michel Kocher, ‡Nikil Jayasheelan, ‡Jagannath Kamath
anu_shaju_ec13f06@nitk.edu.in, sumam@nitk.edu.in, michel.kocher@heig-vd.ch
*Department of ECE, National Institute of Technology Karnataka, Surathkal, India
†La Haute Ecole d'Ingnierie et de Gestion du Canton de Vaud (HEIG-VD), Switzerland
‡Department of Orthopaedics, Kasturba Medical College Hospital Mangalore, Karnataka, India

***Abstract*—Osteoporosis is a disease caused by reduction of bone mass, bone strength and deterioration of bone structure. The gold standard method for diagnosis of osteoporosis is measurement of bone mineral density (BMD) using Dual X-ray Absorptiometry (DXA). However, DXA is expensive and not widely available in developing countries. An alternative cost-effective method for measurement of bone loss and strength is metacarpal radiogrammetry, by which geometric measurements of cortical bone of the metacarpal bone are measured. In this paper, we propose a fully automated method for segmentation of third metacarpal bone from hand radiograph and radiogrammetric measurements using mathematical morphology. Cortical width and thickness are measured from the endosteal and periosteal edges of the metacarpal bone using which bone indices which help in diagnosis of osteoporosis can be computed. The proposed segmentation method was tested on 157 hand X-ray images. A success rate of 94.9% is obtained for automatic detection of third metacarpal bone. Evaluation of cortical measurements of 3 calibrated images is done by comparing the results with ground truth. The mean accuracy error obtained was 0.02cm and 0.04cm for cortical width and medullary width, respectively.**

***Index Terms*—Osteoporosis, Radiogrammetric measurements, Metacarpal bone, Mathematical morphology, Watershed segmentation.**

I. Introduction

Osteoporosis is a disease characterized by low bone mass and structural deterioration of bone tissue, leading to bone fragility and an increased susceptibility to fractures of hip, spine and wrist. The condition often remains painless and undiagnosed until a fragility fracture occurs. According to World Health Organisation (WHO), osteoporosis is second only to cardiovascular diseases as a global health problem. Statistics show that in 2012, the number of osteoporotic cases in India was around 55 million (4%) and by 2022, it is expected to rise to 75 million (5%) [1].

The gold standard technique used for diagnosis of osteoporosis and fracture prediction is determination of bone mineral density (BMD) using Dual Energy X-ray Absorptiometry (DXA). Even though measurement using DXA is accurate and highly precise and has low radiation dose, the cost of DXA scans and availability of DXA system are major limiting factors in developing economies. The cost of DXA scan ranges between Rs.1800 to 4500 [2]. Hence, there is a need for a low cost method for the early diagnosis of osteoporosis and fracture risk assessment.

978-1-5090-1746-1/16/$31.00

An alternative simple low cost technique for measurement of bone loss from radiographs is radiogrammetry. It is a manual method by which geometric measurements of the cortical bone such as cortical width, cortical thickness, cortical area, length of the bone, etc. are measured from a radiograph. Bone indices derived from these measurements such as Combined Cortical Thickness (CCT), Metacarpal Index (MCI), Exton-Smith Index (ESI), Pediatric Bone Index (PBI), etc. are used to diagnose osteoporosis [3].

The main limitation of conventional radiogrammetry is that manual measurement is time-consuming and suffer from subjective error and inter-observer variability. Precision and reproducibility of manual segmentation is poor. To overcome this, various automated methods for radiogrammetric measurements have evolved [4], [5]. Since osteoporosis is a systemic disease in which bone loss occurs in the whole body, measurement of bone loss in any part of the skeletal body reflects the bone loss at all other parts. Hence, radiogrammetric measurements from metacarpal bone of hand can be used to measure the bone loss at any skeletal site [6]. Computerised metacarpal radiogrammetry requires automatic segmentation of the metacarpal bone and automatic measurement of the cortical bone dimensions. Automatic segmentation reduces subjective error and measurement time. It has high precision and reproducibility if the image has a high resolution and high signal to noise ratio. In this paper, we develop a fully automated method for segmentation of third metacarpal bone and computation of radiogrammetric measurements from hand radiographs.

This paper is organised as follows: Section II gives an overview of segmentation methods used in metacarpal bone segmentation. Section III describes our proposed method for the automatic extraction of the third metacarpal bone and measurement of cortical bone geometry. Experimental results and comparison with state-of-art methods are explained in Section IV. Section V gives a summary of the paper.

II. Background

A. Segmentation Approaches

Several segmentation approaches are being used for the automatic segmentation of metacarpal bones from hand ra-

diographs. Most of the methods are based on deformable models. Active Contour model, also known as Snake, is the simplest deformable model-based technique. Garcia et. al. [7] developed a truncated Snake model for the segmentation of metacarpal and phalanx bones of hand and a success rate of 73.9% was achieved. Low quality and over-exposed images produced poor segmentation results.

Digital X-ray Radiogrammetry (DXR) [8] is a computerised radiogrammetric technique that uses Active Shape Model (ASM) to automatically segment the metacarpal bones from hand radiographs. ASM is a parametric deformable model where a mean shape model of the global shape variation of the metacarpal bone is built from the manually annotated training datasets, by first aligning the shapes by translation, scaling and rotation and then using Principal Component Analysis (PCA) to describe the variation of the aligned shapes among individuals. Finally, the mean shape is used to fit the model to the test image. A success rate of 99.5% is reported.

Active Appearance Model (AAM) [9] combines a statistical shape model and gray level appearance of the object. It is more robust than ASM. However, AAM requires a large set of training images and is slower than ASM. In order to improve the accuracy and computation time of AAM, Langs et. al. [10] used Active Feature Model (AFM) to segment metacarpal and phalanx. This model analyzed both shape and texture features during the training phase. It was faster and more accurate than AAM. The mean error achieved was 3.56 pixels. However, the training phase requires manual annotations.

L. Fischer [11] used Shape Particle Filter (SPF) to extract metacarpal bones. It has proved to be more robust than ASM and AAM. The mean landmark error obtained was 18.2 pixels. However, the precision and accuracy was poor and it took longer computation time than ASM and AAM.

A.J. Raheja [12] segmented metacarpal bones using medial axis transform (MAT) and watershed algorithm. Success rate of 75% was achieved and measurement accuracy of 0.5% was obtained. High inter- and intra-observer agreement of 92% and 96% was achieved, respectively. However, this method failed for low quality and over-exposed images.

The accuracy and success rate of segmentation of metacarpal bones using ASM depends on the training dataset. Creating a large number of manually annotated datasets for the training phase is a tedious task. Hence, there is a need for a simple and accurate automatic segmentation method for metacarpal bones from hand radiographs.

In this paper, we develop a simple and efficient fully-automated segmentation method for extraction of third metacarpal bone and to automatically determine cortical measurements from the hand radiographs. Watershed segmentation using markers is used in the proposed approach to detect the periosteal and endosteal edges of the third metacarpal bone.

B. Watershed Segmentation

Watershed segmentation [13] is fast and accurate and does not require a training phase. It interprets an image as a topographic surface where the intensity levels represent altitudes.

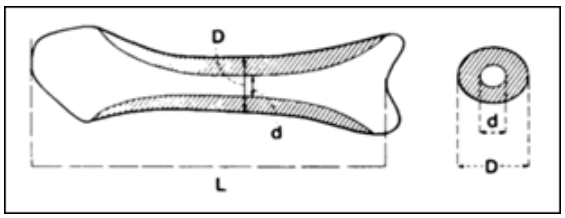

Fig. 1. Cortical measurements [14]

Water is thought of as being flood into the surface from the local minima points to fill up the catchment basin regions. In order to prevent the overflow of water from one catchment basin to the other, watershed lines are created. The watershed lines represent the boundary of the regions. A major limitation is that the resultant image may be over-segmented. This is due to the presence of noise or a large number of local minima in the image. Over-segmentation problem can be alleviated by using marker-controlled watershed segmentation. Markers can be placed at certain regions to level-out the local minima. These markers will act as the local minima and watershed segmentation is done.

C. Metacarpal Radiogrammetry

Metacarpal radiogrammetry [6] is the technique by which cortical measurements are taken from third metacarpal bone using hand radiograph. The different measurements taken from metacarpal bone are cortical width, D, medullary width, d and length of metacarpal bone, L, as shown in Fig.1. Other measurements obtained from radiogrammetric analysis are combined cortical thickness T and cortical area A [3], defined as

$$T = D - d \tag{1}$$

$$A = \pi T D(1 - \frac{T}{D}) \tag{2}$$

III. Proposed Methodology

The proposed segmentation method is based on mathematical morphology [15] and watershed segmentation. The proposed approach consists of four main stages: 1) Preprocessing, 2) Automatic marker placement, 3) Automatic segmentation of third metacarpal bone and 4) Radiogrammetric measurements. In stage 1, the input image is denoised and calibrated with a standard device of known size. In stage 2, bone region is extracted from the hand radiograph using mathematical morphology and the third metacarpal bone is located automatically. In stage 3, marker-controlled watershed segmentation is used to detect periosteal (outer) and endosteal (inner) edges of the metacarpal bone. Finally in stage 4, cortical measurements are determined from the segmented bone. A block diagram of the proposed method is shown in Fig 2.

A. Preprocessing

X-ray images pose various challenges for segmentation and accurate geometric measurements. Hence preprocessing of X-ray images is an essential preliminary step for segmentation.

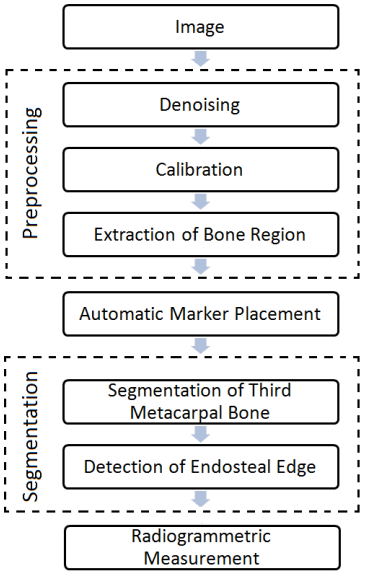

Fig. 2. Flowchart of proposed segmentation approach

The various challenges of X-ray imaging are blurring due to finite size of X-ray source and patient motion, contrast variation due to X-ray exposure conditions, magnification effects, etc.

In order to remove noise in X-ray images, non-local mean [16] is used. Non-local mean method helps to preserve the edges while removing the noise and thus helps to produce a good gradient image for the watershed method.

The magnification effect in X-ray image can be overcome by using a calibration device of known size. The use of a standard calibration material can help to standardize the radiographs and improve the accuracy of cortical measurement. In this work, calibration device is placed on top corner of X-ray image during image acquisition. In order to extract it from the image, the denoised image is thresholded using Otsu method [17]. The upper half of the binary image is eroded with a large disk-shaped structuring element. The largest connected component is taken and reconstructed to extract the device and its size is measured in pixels. Since the actual size of the device is known, dimension of image pixel can be determined as

$$Pixel\ dimension = \frac{Actual\ diameter\ (cm)}{Measured\ diameter\ (pixels)} \quad (3)$$

B. Automatic Marker Placement and Segmentation

The denoised image can be thresholded using Otsu method. But in some cases, it may fail to detect the proximal phalanx bones as foreground, due to under-exposure. Since bone region has a higher intensity than soft tissue, bone can be extracted using open top hat residue analysis of the X-ray image with a large disk structuring element as shown in Fig 3(b). The resultant image is then thresholded using Otsu threshold in order to get a binary image of the bone region. However, this image may contain disconnected bones at the wrist region. Hence, the union of thresholded denoised image using Otsu

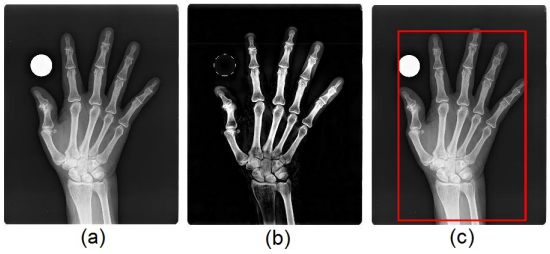

Fig. 3. Extraction of hand: (a) Original image, (b) Open top hat transform, (c) Bounding box of hand

and thresholded open top hat is taken as the binary image. The largest connected component is extracted to get the hand and the bounding box is detected, as shown in Fig 3(c).

In order to automatically locate an internal marker for detection of third metacarpal bone, the binary image of hand bone region is masked over the grayscale image. Line profiles are determined for rows spaced at equal intervals in the lower half of this extracted grayscale bone image. The row profiles passing through metacarpal region shows peaks with greater deviation when compared to the carpal region, as shown in Fig 4(a) and (b). The row having the maximum standard deviation of peaks in the line profile will pass through the metacarpal region, containing all 5 metacarpals. In the binary hand bone image, 5 largest objects along this corresponding row are labeled, from which the third object positioned from the left or right acts the internal marker of the third metacarpal bone.

With respect to the internal marker and bounding box of hand, a rectangular external marker is determined. The external marker is fixed to lie within 10% of the hand border on either side and 20% of the hand border on the upper and lower side of the internal marker, as shown in Fig 5(a). The gradient image used for the segmentation is the sum of increasing scale dilations of morphological gradient of image. This ensures that the edges of metacarpal bone are linked together. Marker-controlled watershed segmentation is applied on the gradient function to extract the third metacarpal boundary (periosteal edge), as shown in Fig 5(b).

For the detection of endosteal edge of bone, the segmented periosteal edge is used as external marker. Watershed region of the segmented cortical bone is eroded by large disk structuring element to form internal marker, as shown in Fig 5(c). The grayscale bone image is transformed by open top hat using

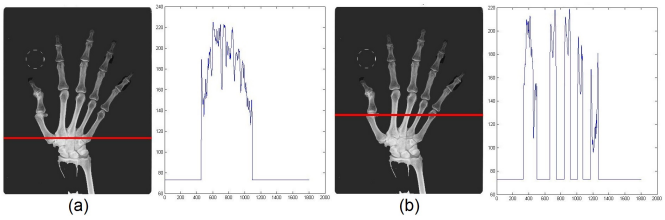

Fig. 4. Line profile of (a) Carpal region and (b) Metacarpal region

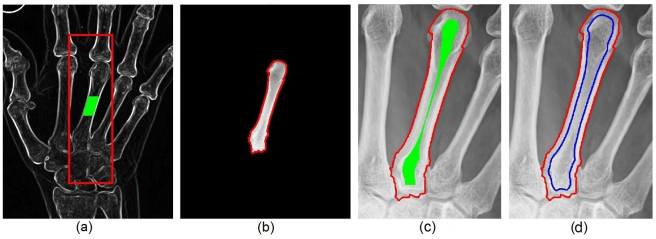

Fig. 5. Segmentation using watershed: (a) Gradient image with markers, (b) Segmented third metacarpal, (c) Markers for detection of endosteal edge, (d) Detected endosteal edge

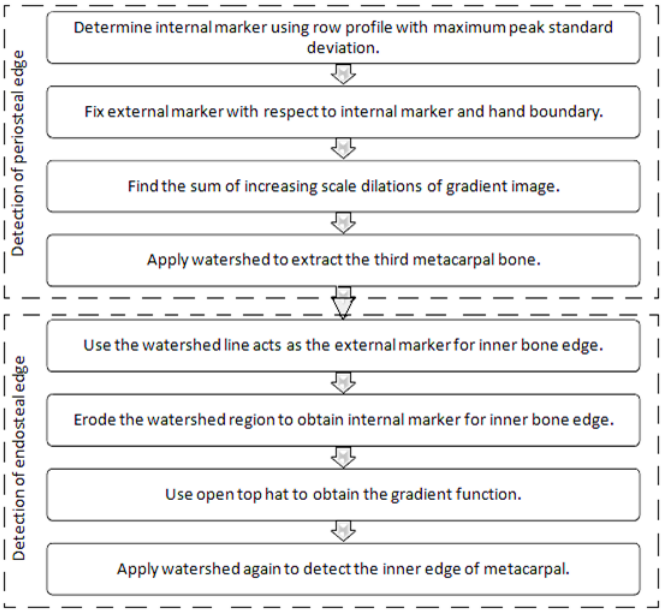

Fig. 6. Flowchart of the automatic segmentation

rectangular structuring element to get the gradient image for endosteal edge. Since the metacarpal bone is elongated vertically, rectangular structuring element produces a better gradient image than disk-shaped structuring element. Segmentation of trabecular bone is obtained by applying marker-controlled watershed to the segmentation function as shown in Fig 5(d). Fig 6 shows the flowchart of the automatic segmentation of periosteal and endosteal edges of the third metacarpal bone.

C. Radiogrammetric Measurements

For measurement of cortical thickness and width, the extracted metacarpal bone is aligned vertically. Radiogrammetric measurements are taken from the shaft of the metacarpal bone as shown in Fig 7. A region of interest (ROI) region for the measurements is placed at the shaft of bone by discarding the head and base regions of the metacarpal bone. Cortical measurements are determined in number of pixels and converted to units in cm using the pixel dimension determined from calibration device. Cortical width is the total diameter of the bone, measured by finding the distance between periosteal

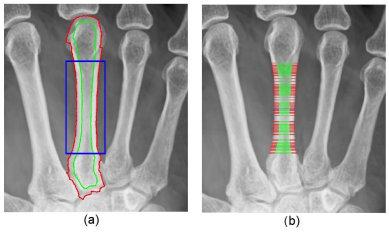

Fig. 7. Radiogrammetric measurements: (a) Detection of bone shaft, (b) Cortical measurements

edges. Medullary width is the diameter of the trabecular bone, corresponding to the distance between endosteal edges. The difference between the cortical and medullary widths gives the cortical thickness. To find medial and lateral cortical thickness separately, the central axis of bone shaft is determined using morphological skeleton by thinning the extracted third metacarpal bone.

IV. Results

A. Datasets

149 images were taken from publicly available dataset provided by Image Processing and Informatics Lab, University of Southern California [18], which consist of left hand Anterior-Posterior (AP) view radiographs of healthy subjects of age group 17-18 years. Hand radiograph of 8 people (4 healthy and 4 osteoporotic) imaged with calibration device at Kasturba Medical College, Mangalore, Karnataka, India, were also used. The data consists of both left and right hand AP view radiographs.

B. Simulation Results

The proposed method was implemented using Matlab 2015a and SDC Morphology Toolbox. Automatic extraction and segmentation of third metacarpal bone using the proposed method was performed on the hand radiographs. Cortical measurements determined automatically from the third metacarpal bone of calibrated hand X-ray images are shown in Table I. Combined cortical thickness (CCT) and cortical area (CA) have been determined from the measured average values of cortical width (CW) and medullary width (MW) of bone shaft.

C. Validation with Ground Truth

Validation of the cortical measurements obtained using the proposed automatic segmentation approach has been done using ground truth provided by orthopaedicians for 3 calibrated X-ray images. The percentage error in cortical measurements from proposed method and ground truth are given in Table II. Segmentation results shows a mean error of 0.02cm (1 pixel) for cortical width and 0.04cm (2 pixels) for medullary width.

D. Comparison with other segmentation techniques

The proposed segmentation method was tested on 157 images. It automatically detected and segmented the third metacarpal bone in 149 images. A success rate of 94.9% was thus obtained for the automatic detection of third metacarpal

TABLE I
CORTICAL MEASUREMENTS OF THIRD METACARPAL BONE

Data	Age	Pixel dimension (cm)	CW (cm)	MW (cm)	CCT (cm)	CA (cm^2)
1	26	0.023	0.92	0.65	0.27	0.55
2	40	0.01	0.88	0.53	0.34	0.57
3	40	0.01	0.99	0.63	0.35	0.7
4	42	0.022	0.97	0.64	0.33	0.66
5	62	0.01	0.87	0.69	0.19	0.4
6	64	0.027	0.84	0.5	0.35	0.54
7	70	0.01	0.8	0.56	0.24	0.43
8	80	0.01	0.81	0.55	0.27	0.46

TABLE II
COMPARISON OF MEASURED CORTICAL VALUES WITH GROUND TRUTH

Data	Pixel dimension (cm)	Actual CW (cm)	Measured CW (cm)	Error (%)	Actual MW (cm)	Measured MW (cm)	Error (%)
1	0.022	0.93	0.93	0.0	0.59	0.56	5.1
		0.81	0.78	3.7	0.45	0.48	-6.7
		0.82	0.82	0.0	0.43	0.54	-25.6
2	0.023	1.07	1.09	-1.9	0.72	0.7	2.8
		0.91	0.94	-3.3	0.56	0.55	1.8
		0.81	0.81	0.0	0.42	0.42	0
3	0.027	0.89	0.81	9.0	0.41	0.36	12.2
		0.74	0.73	1.4	0.23	0.27	-17.4
		0.75	0.7	6.7	0.27	0.3	-11.1

TABLE III
COMPARISON OF SUCCESS RATE OF METACARPAL DETECTION

Author	Method	Success rate	Test images
Garcia et. al. [7]	Snake	73.9%	59
Thodberg et. al. [8]	ASM	99.5%	5000
Raheja [12]	MAT, Watershed	75%	357
Proposed method	Watershed	94.9%	157

bone. Table III compares the success rate of the proposed approach with other techniques. Our method outperforms Snake and watershed transform with MAT in terms of detection of metacarpal bone. ASM shows high success rate due to large training dataset used.

Using the proposed method, segmentation result was poor for images with very low contrast. Contrast variation affects the gradient image, which in turn reduces the accuracy of edge detection. Segmentation accuracy can be increased by developing improved contrast enhancement and edge detection techniques.

V. CONCLUSION

In conclusion, a fully-automatic method was developed for the extraction of third metacarpal bone and detection of periosteal and endosteal edges from hand radiographs using watershed algorithm. The proposed method showed a success rate of 94.9% in accurate detection of third metacarpal bone when tested on 157 hand X-ray images. Cortical measurements were measured automatically, using which bone indices like Metacarpal Index, Exton-Smith Index, Pediatric Bone Index, etc. that give a measure of bone loss and bone strength, can be computed. The results obtained for 3 calibrated hand X-ray images were compared with ground truth and mean accuracy error of 0.02cm and 0.04cm was obtained for cortical width and medullary width, respectively. This method outperformed other state-of-art methods in terms of success rate for detection of metacarpal bone. The results obtained with the proposed approach are promising. Therefore, metacarpal radiogrammetric measurements determined from a large dataset can be used for the diagnosis of osteoporosis.

REFERENCES

[1] Choosing a Clinical Centre for a Bone/Joint Health Human Study-www.naturalproductsinsider.com/articles/2013/08/choosing-a-clinical-center-for-a-bone-joint-healt.aspx.

[2] Asia-Pacific Regional Audit on Epidemiology, Costs and Burden of Osteoporosis in 2013-www.iofbonehealth.org/data-publications/regional-audits/asia-pacific-regional-audit.

[3] H. Thodberg, R. Van Rijn, T. Tanaka, D. Martin, and S. Kreiborg, "A paediatric bone index derived by automated radiogrammetry," *Osteoporosis Int.*, vol. 21, no. 8, pp. 1391–1400, 2010.

[4] G. S. Seo, M. Shiraki, C. Aoki, J.-T. Chen, J. Aoki, K. Imose, Y. Togawa, and T. Inoue, "Assessment of bone density in the distal radius with computer assisted X-ray densitometry (CXD)," *Bone and Mineral*, vol. 27, no. 3, pp. 173–182, 1994.

[5] N. Shankar, V. Sapthagirivasan, A. Vijay, K. Kirthika, and M. Anburajan, "Evaluation of osteoporosis using radiographic hip geometry, compared with dual energy X-ray absorptiometry (DXA) as the standard," in *Int. Conf. Systems in Medicine and Biology (ICSMB)*. IEEE, 2010, pp. 259–264.

[6] A. Rosholm, L. Hyldstrup, L. Baeksgaard, M. Grunkin, and H. Thodberg, "Estimation of bone mineral density by digital X-ray radiogrammetry: theoretical background and clinical testing," *Osteoporosis Int.*, vol. 12, no. 11, pp. 961–969, 2001.

[7] D. Luis-Garcia, M. Martin-Fernández, J. I. Arribas, C. Alberola-López *et al.*, "A fully automatic algorithm for contour detection of bones in hand radiographs using active contours," in *Proc. 2003 Int. Conf. Image Processing (ICIP)*, vol. 3. IEEE, 2003, pp. 418–421.

[8] H. H. Thodberg and A. Rosholm, "Application of the active shape model in a commercial medical device for bone densitometry," *Image and Vision Computing*, vol. 21, no. 13, pp. 1155–1161, 2003.

[9] T. F. Cootes, G. J. Edwards, and C. J. Taylor, "Active appearance models," *IEEE Trans. Pattern Analysis and Machine Intelligence*, no. 6, pp. 681–685, 2001.

[10] G. Langs, P. Peloschek, R. Donner, M. Reiter, and H. Bischof, "Active feature models," in *18th Int. Conf. Pattern Recognition (ICPR)*, vol. 1. IEEE, 2006, pp. 417–420.

[11] L. Fischer, "Using shape particle filters for robust medical image segmentation," Tech. Report- Vienna University of Technology, Tech. Rep., 2009.

[12] A. J. Raheja, "Automated analysis of metacarpal cortical thickness in serial hand radiographs," Ph.D. dissertation, Wright State University, 2008.

[13] F. Meyer, "Topographic distance and watershed lines," *Signal processing*, vol. 38, no. 1, pp. 113–125, 1994.

[14] A. L. Huddleston, *Quantitative methods in bone densitometry*. Springer Science & Business Media, 1988.

[15] P. Soille, *Morphological image analysis: Principles and Applications*. Springer Science and Business Media, 2013.

[16] A. Buades, B. Coll, and J.-M. Morel, "A non-local algorithm for image denoising," in *IEEE Computer Society Conf. Computer Vision and Pattern Recognition (CVPR)*, vol. 2. IEEE, 2005, pp. 60–65.

[17] N. Otsu, "A threshold selection method from gray-level histograms," *Automatica*, vol. 11, no. 285-296, pp. 23–27, 1975.

[18] H. Huang, A. Zhang, B. Liu, Z. Zhou, J. Documet, N. King, and L. Chan, "Data grid for large-scale medical image archive and analysis," in *Proc. 13th Annual ACM Int. Conf. on Multimedia*, 2005, pp. 1005–1013.